Total (elastic + absorption) cross sections for e-CH_4 collisions in a spherical model at 0.10—500 eV

Ashok Jain
Physics Department, Cardwell Hall, Kansas State University, Manhattan, Kansas 66506
(Received 9 June 1986)

Electron-CH_4 scattering is investigated in a wide energy range (0.1—500 eV) by using a previously proposed spherical model [A. Jain, J. Chem. Phys. **81**, 724 (1984)]. The study is divided into three energy regions: the 0.1—1.0-eV region, where a well-known minimum occurs in the total cross section [Ramsauer-Townsend (RT) effect], between 2 and 20 eV, with a d-wave broad structure around 7—8 eV, and from 20 to 500 eV, where inelastic channels (mainly ionization and dissociation) dominate over the elastic process. It is shown that a simple model, in which the total optical complex potential is spherical, is capable of reproducing qualitative features in the total, differential, and momentum-transfer cross sections in the present energy region. The present results are almost equivalent to more rigorous close-coupling calculations at low energies ($E < 20$ eV), where the rotationally elastic channel dominates. Below 20 eV, the total optical potential is real and consists of three spherical terms, namely, a static term calculated accurately from near-Hartree-Fock one-center methane wave functions, a parameter-free polarization potential of Jain and Thompson (however, below 1 eV we employ a cutoff-type phenomenological polarization potential), and a local-exchange interaction in the asymptotically adjusted version of the Hara free-electron-gas exchange (AAHFEGE) potential (however, below 1 eV, we consider just the HFEGE form). At and above 20 eV, we employ a complex optical potential with the same real part as in the 2—20-eV region, while the imaginary part is an energy-dependent absorption potential calculated from target electron density and short-range static-exchange potential in the quasifree model with Pauli blocking [Staszewska *et al.*, J. Phys. B **16**, L281 (1983)]. Two versions of this absorption potential are used; one with undistorted charge density and the other with a polarized density. The final complex total optical potential is treated exactly in a partial-wave analysis to yield various cross sections. The results are compared with the available experimental and other theoretical data. The absorption cross sections are not sensitive to various forms of real part of the optical potential, and in general, reduce the elastic cross sections significantly.

I. INTRODUCTION

Recently we proposed a simple spherical model[1,2] to study elastic scattering of intermediate- and high-energy (20—500-eV) electrons (positrons) by methane molecules. In this model, the total optical potential of electron-CH_4 system is approximated by a sum of three terms: a static potential generated without additional approximations from near-Hartree-Fock one-center methane wave functions with a large basis set; an exchange term in the free-electron-gas exchange (Hara[3] type) (HFEGE) approximation; and a parameter-free energy-independent (however nonadiabatic) polarization interaction of Jain and Thompson:[4,5] We retained only the spherical term ($l=0$), in the one-center expansion of all the three interactions belonging to A_1 irreducible representation of CH_4 point group. In addition, this optical potential was pure real, thus allowing no loss of flux due to electronically inelastic, dissociation and ionization channels, which become open above 10—15 eV. In some special cases, where the coupling between the angular momentum of the electron and the rotational motion of the molecule is weak, this simple truncation only up to the $l=0$ term may be justified, since the methane molecule has no dipole or quadrupole moments, and the higher-order moments contribute very little to the total (rotationally summed) cross sections. Note that such an approximation is not true for other molecules such as H_2, N_2, CO_2, H_2O, NH_3, etc. The final optical potential was treated exactly in a partial-wave analysis to extract integral (σ_i), momentum-transfer (σ_m) and differential (DCS's) cross sections. The results were found in good accord with existing experimental data in the considered range of 20—500 eV.[2] In this energy region, only two previous calculations were available: one due to Buckingham *et al.*[6] at 6—50 eV for the σ_i and DCS, by using a self-consistent field for CH_4 without including exchange and polarization effects; Dhal *et al.*[7] employed a less accurate model in the eikonal approximation without including exchange interaction. We would not include these calculations in our comparison here due to obvious reasons.

However, our earlier attempt[2] is incomplete in several ways. First, the total optical potential is real, which gives only elastic cross sections at intermediate and high energies. In this article, we have tried to evaluate total (absorption plus elastic) (σ_t) cross sections by introducing an approximate absorption potential in the form of an imaginary part of the complex optical potential. The corresponding phase shifts are complex and the σ_t can now be compared directly with the measurement of electron-transmission-spectroscopy (ETS) type experiments. A

 ©1986 The American Physical Society

wealth of experimental data on the σ_t are available from the early thirties[8-11] to very recent ones[12-20] in a wide energy range (0.1—800 eV). However, there is a paucity of theoretical calculations on this system. Above 20 eV, there is no single calculation on the σ_t. Since at low energies ($E < 20$ eV) almost all electronically inelastic channels are either very small or closed and vibrational transition cross sections are small too, the close-coupling (CC),[4-5,21-25] continuum multiple scattering (CMS) (Refs. 26—29), and Schwinger multichannel[29] calculations on the rotationally summed (vibrationally elastic) cross sections can be compared with the experimental σ_t. However all these rigorous calculations still need further improvements (see Gianturco and Thompson[30] and Gianturco and Jain[31]).

Our second goal in this paper is to examine the validity of this simple spherical model below 20 eV. This is desirable, since in the 0—20-eV region, there is an enhancement in the σ_t around 7—8 eV due to d-wave scattering, which is dominant in the T_2 symmetry of the e-CH_4 system[21] and a well-known minimum [Ramsauer-Townsend (RT) effect] occurs at 0.4—0.5 eV. In addition, there are some discrepancies among the existing experimental data particularly below 20 eV. Here, we examine various spherical models and show that the static-exchange (HFEGE asymptotically adjusted)-polarization (Jain-Thompson[4]) (SEAPJT) model (for all notations in the following see the Appendix) is quite capable to reproduce the 7—8-eV structure in accord with experimental data and the RT minimum can be reproduced satisfactorily by tuning a parameter-dependent polarization potential (Gianturco-Thompson type[21]) [(SEPGT) model]. (The imaginary part of the optical potential is not important in this region.) It is interesting to note here that the present results in the 0—20-eV region are very close to previously reported close-coupling calculations[4,5,21-25] and in some cases even better if a suitable combination of the exchange and the polarization potentials is fed into the scattering equation (see later text). However, comparison with recent static exchange[29] (in which exchange is treated exactly via Schwinger-multichannel theory) calculations would be interesting in order to access the role of model-exchange potentials.

The present calculations involve no adjustable parameter above 1 eV. All the scattering parameters are evaluated from complex phase shifts calculated in the variable-phase approach (VPA). There are numerous measurements, from very old[32-35] to recent ones,[36-41] on the DCS for e-CH_4 elastic scattering. These experimental angular functions have been used to estimate the σ_m:[37-41] the σ_m have also been extracted from swarm data analysis.[42-44] Tice and Kivelson[45] have obtained σ_m at thermal energies from their cyclotron resonance experiment. Our calculations on the DCS and the σ_m will be compared with these available experimental data.

The only visible effect of neglecting higher-order terms in the expansion of the optical potential is seen in the DCS around middle angles at energies below 50 eV, where a sharp dip contradicts with the shallow structure observed in experiments and to some extent in the close-coupling calculations also. This is obvious, since considering only the spherical term means neglecting higher-order rotational excitations (from $J=0$ to $J'=3$, 4, and so on in the case of CH_4). The rotationally inelastic DCS's for $\Delta J \neq 0$ vary slowly with angle and are larger than the elastic ($\Delta J = 0$) DCS's around 110°—120°; thus, making the DCS's shallow at these angles. This is further confirmed by the rotationally elastic and inelastic measurements of Müller *et al.*,[46] where the elastic cross sections show a deep minima in fair agreement with the present and the CC results of Jain and Thompson.[5]

For the absorption potential, we invoke a quasifree scattering model using Pauli blocking as derived and used for electron scattering by Truhlar and co-workers.[47] This energy-dependent absorption potential is a function of static (plus exchange) potential and the target charge density. We, however, make this potential more flexible by using both the undistorted and the distorted charge densities (the later quantity was calculated approximately in the presence of incoming field of the projectile[48]). Results are compared using both the densities: It is found that an absorption potential using the distorted charge density is more successful. The elastic cross sections are reduced by including the imaginary part in the optical potential. The absorption cross-section curve is peaked around 100 eV and dominates over the elastic curve about this energy.

Another reason to perform the present theoretical calculations on the e-CH_4 system, is the need of such data in various applied sciences.[49,50] The low-energy e-CH_4 scattering cross sections are required in optimization of the characteristics of diffuse discharges switches;[49] experiments indicate that the CH_4 provides the best e-beam switch performance.[50] Many proportional and drift counters contain CH_4 gas and there have been several attempts to explain some aspects of the behavior of these devices in terms of electron scattering data for the filling gas[51,52] analysis. The methane gas has been found in many astrophysical objects such as the Uranus and Neptune.[53]

The rest of the paper is organized as follows. In Sec. II, we give a brief summary of the present theory and numerical procedure. The results are discussed separately in three energy regions: 0.1—1.0, 2—20, and 20—500 eV in Sec. III. Some concluding remarks are presented in Sec. IV. Atomic units are used throughout in this paper.

II. THEORY

A general description of the present spherical model is given in our previous papers.[1,2] In brief, the total interaction between an electron and the CH_4 molecule is represented by an optical potential $V_{\text{opt}}(\mathbf{r})$. This optical potential is expanded around the central (carbon) atom in terms of symmetry-adapted functions of A_1 symmetry (totally symmetric), i.e.,

$$V_{\text{opt}}(\mathbf{r}) = \sum_{l,h} V_{lh}(r) X_{lh}^{A_1}(\hat{\mathbf{r}}) .$$

In our spherical approximation, only first term ($l=0$, $h=1$) is retained. In the following $V_{01}(r)$ is denoted simply by $V_{\text{opt}}(r)$.

In a usual potential scattering problem, the following

differential equation is solved for the scattered electron function at energy k^2, i.e.,

$$\left[\frac{d^2}{dr^2}+k^2-\frac{l(l+1)}{r^2}-V_{\text{opt}}(r)\right]f_l(kr)=0\ , \tag{1}$$

where $V_{\text{opt}}(r)$ is the complex optical potential for the e-CH_4 system given by

$$V_{\text{opt}}(r)=V_R(r)+iV_{\text{abs}}(r)\ . \tag{2}$$

The real part $V_R(r)$ is represented by three spherical local terms, namely

$$V_R(r)=V_{\text{st}}(r)+V_{\text{ex}}(r)+V_p(r)\ , \tag{3}$$

where $V_{\text{st}}(r)$ is the static potential calculated accurately from near-Hartree-Fock one-center CH_4 wave functions[54] with a large basis set (14 functions of a_1-type and 23 of t_2-type orbitals). The exchange potential $V_{\text{ex}}(r)$ is the HFEGE potential[55]

$$V_{\text{ex}}(r)=\frac{2}{\pi}k_f(r)\left[\frac{1}{2}+\frac{1-n}{4n}\ln\left|\frac{1+n}{1-n}\right|\right] \tag{4}$$

with

$$k_f(r)=[3\pi^2\rho_0(r)]^{1/3} \tag{5a}$$

and

$$n(r)=(k^2+2I+k_f^2)^{1/2}/k_f\ . \tag{5b}$$

Here I is the ionization potential of the CH_4 molecule, $\rho_0(r)$ is the undistorted charge density of the target. Above 1 eV, we use an asymptotically adjusted version of HFEGE by setting $I=0$ in Eq. (6); this is denoted by AAHFEGE. The third term in Eq. (3), $V_p(r)$, is the polarization potential. Above 1 eV we found that a parameter-free approximate polarization potential of Jain and Thompson[4] (along with the AAHFEGE potential) is more successful (explicit expressions for this potential in the present spherical model are given earlier).[2] This term is denoted by the JT potential. However, below 1 eV, the JT potential is quite weak and unable to reproduce the RT minimum around 0.4–0.5 eV (along with either the HFEGE or the AAHFEGE potentials).[23,24] In this case, we employ a usual phenomenological form,[21,22]

$$V_p(r)=-(\alpha_0/2r^4)[1-\exp(-r/r_c)]^6\ , \tag{6}$$

where α_0 is the static polarizability of methane [$\alpha_0=17.5$ a.u. (Ref. 56)] and r_c is chosen by adjusting the position of the RT minimum in the total cross section: A value of 1.175 a.u. for r_c, calculated recently by us,[23] is used in Eq. (6). This polarization model is represented as the Gianturco and Thompson (GT) model. All the three potentials are shown earlier in Fig. 1 of Ref. 23.

For the imaginary part of the optical potential $V_{\text{abs}}(r)$, we use the absorption potential discussed by Truhlar and co-workers.[47] This is written as

$$V_{\text{abs}}(r)=-\rho(r)(v_{\text{loc}}/2)^{1/2}(8\pi^2/10k_f^3E)\times H(2k^2-k_f^2-2\Delta)(A_1+A_2+A_3)\ , \tag{7}$$

where

$$v_{\text{loc}}(r)=k^2-V_{\text{st}}(r)-V_{\text{ex}}(r)\ , \tag{8a}$$

$$A_1=5k_f^3/2\Delta\ , \tag{8b}$$

$$A_2=-k_f^3(5k^2-3k_f^2)/(2k^2-k_f^2)^2\ , \tag{8c}$$

$$A_3=2H(2k_f^2+2\Delta-2k^2)(2k_f^2+2\Delta-2k^2)^{5/2}\ . \tag{8d}$$

Here $H(x)$ is a Heaviside function defined by

$$H(x)=\begin{cases}1, & x\geq 0\\ 0, & x<0\ ,\end{cases} \tag{9}$$

and Δ is the mean excitation energy calculated from the expression

$$\Delta=\frac{2\langle\psi_0|z^2|\psi_0\rangle}{\alpha_0}\ , \tag{10}$$

where $|\psi_0\rangle$ is the ground state of the target molecule. From our one-center wave functions we obtain Δ to be 17.88 eV. As mentioned earlier, we use two versions of V_{abs}, i.e., V_{abs}^0 and V_{abs}^1, corresponding to undistorted $[\rho_0(r)]$ and the distorted $[\rho_1(r)]$ charge densities, respectively, in Eq. (7). The latter quantity has already been discussed by Jain and Thompson.[48] In the following we give only a brief account of this quantity. The polarized charge density is generated approximately from the expression,

$$\rho_1(r_1)=2N\int\psi_0\psi_1\,dr_2\,dr_3\cdots dr_N+\rho_0(r_1)\ , \tag{11}$$

where N is the total number of target electrons with coordinates $r_1,r_2,\ldots,r_N$ and ψ_1 is a first-order wave function calculated approximately by the method of Pople and

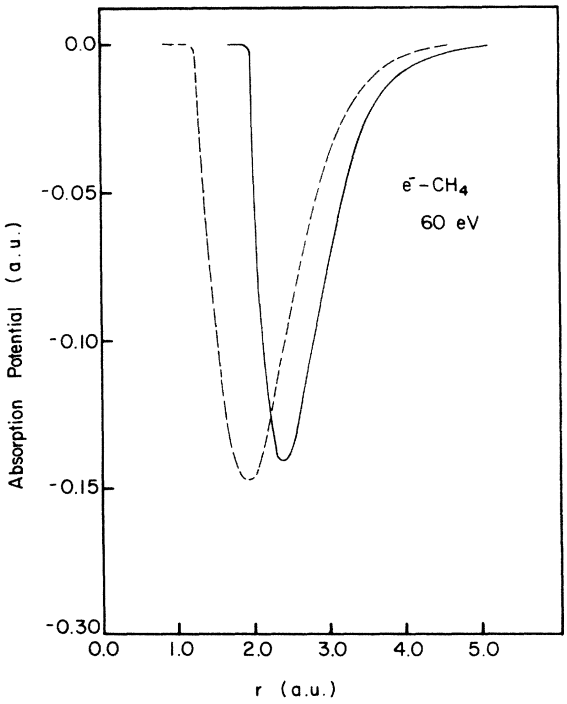

FIG. 1. Absorption potential [Eq. (7)] for the e-CH_4 system at 60 eV: solid curve, using polarized charged density [Eq. (11)]; dashed curve, using undistorted density of the CH_4 molecule.

Schofeld.[57] The distorted charge density is quite different from the undistorted one and gives a different absorption potential. (For the shape of the two densities see Fig. 2 of Ref. 48.) In Figs. 1 and 2 we have illustrated our absorption potentials $V^0_{\rm abs}$ and $V^1_{\rm abs}$ for the e-CH_4 system at two selected energies. The $V^1_{\rm abs}(r)$ is larger at large r values than the $V^0_{\rm abs}(r)$ at all energies and its peak value is smaller than the $V^0_{\rm abs}$ peak value. We shall see later the effects of this difference in the cross sections. Note that the shape of the two sets of curves (Figs. 1 and 2) is similar to each other and also similar to e rare-gas absorption potentials.[47]

In order to solve Eq. (1) for the complex potential we follow the variable-phase approach (VPA).[58] The solution of Eq. (1) gives complex phase shifts for the complex potentials. If $\chi_l(kr)$ and $\bar{\chi}_l(kr)$ are, respectively, the real and imaginary parts of the complex phase-shift function $\delta_l(kr)$, then one can write first-order coupled differential equations in terms of $\chi_l(kr)$ and $\bar{\chi}_l(kr)$. We write these coupled equations in a more convenient way as

$$\chi_l'(kr)=-\frac{2}{k}[2V_R(r)(X^2-Y^2)+2V_{\rm abs}(r)XY] , \tag{12}$$

$$\bar{\chi}_l'(kr)=-\frac{2}{k}[2V_R(r)XY-2V_{\rm abs}(r)(X^2-Y^2)] , \tag{13}$$

where

$$X=\cosh\bar{\chi}_l(kr)[\cos\chi_l(kr)j_l(kr)-\sin\chi_l(kr)\eta_l(kr)] , \tag{14a}$$

$$Y=-\sinh\bar{\chi}_l(kr)[\sin\chi_l(kr)j_l(kr)-\cos\chi_l(kr)\eta_l(kr)] , \tag{14b}$$

and $j_l(kr)$ and $\eta_l(kr)$ are the usual Riccati-Bessel functions.[58] The Eqs. (12) and (13) are integrated up to a sufficiently large r different for different l and k values.

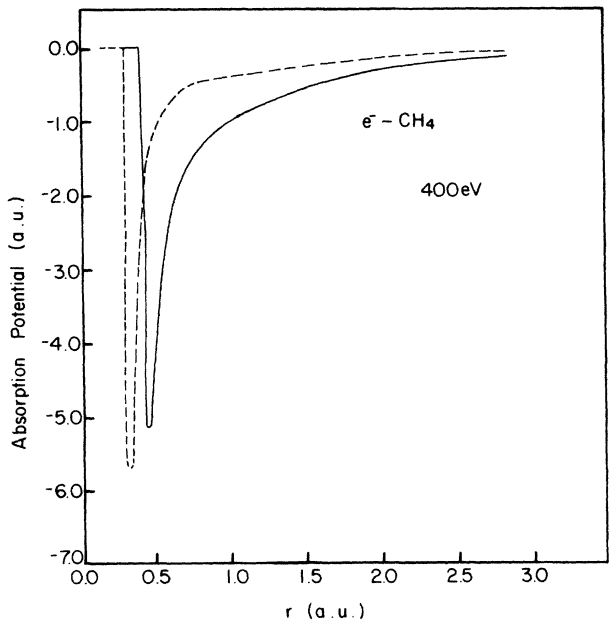

FIG. 2. Same legend as in Fig. 1 but at 400 eV.

The S matrix is written as

$$S_l(k)=\exp(-2\bar{\chi}_l)\exp(i2\chi_l) \tag{15}$$

and the corresponding elastic ($\sigma_{\rm el}$), absorption ($\sigma_{\rm abs}$), and σ_t cross sections can be described in terms of the S matrix,

$$\sigma^l_{\rm el}=\frac{\pi}{k^2}(2l+1)\,|\,1-S_l(k)\,|^2;\quad \sigma_e=\sum_{l=0}^{l_{\max}}\sigma^l_{\rm el} , \tag{16}$$

$$\sigma^l_{\rm abs}=\frac{\pi}{k^2}(2l+1)[1-|\,S_l(k)\,|^2];\quad \sigma_{\rm abs}=\sum_{l=0}^{l_{\max}}\sigma^l_{\rm abs} , \tag{17}$$

$$\sigma^l_t=\frac{2\pi}{k^2}(2l+1)[1-{\rm Re}S_l(k)];\quad \sigma_t=\sum_{l=0}^{l_{\max}}\sigma^l_t . \tag{18}$$

We note that $\sigma_t=\sigma_{\rm abs}+\sigma_{\rm el}$. The DCS are calculated from

$$\frac{d\sigma}{d\Omega}=\frac{1}{4k^2}\left|\sum_{l=0}^{l_{\max}}(2l+1)[S_l(k)-1]P_l(\cos\theta)\right|^2 , \tag{19}$$

where $P_l(\cos\theta)$ is a Legendre polynomial of order l, and the σ_m is evaluated from the integration of Eq. (19) with a weighting factor of $[1-\cos(\theta)]$. The inelasticity or the absorption factor is defined by $|\,S_l(k)\,|=\exp(-2\bar{\chi}_l)$.

III. RESULTS AND DISCUSSION

First we checked the solution of Eqs. (12) and (13) by putting $V_{\rm abs}(r)=0$ and compare the numbers with our earlier calculations;[2] the corresponding VPA phase shifts were in excellent agreement. We also carried out convergence tests with respect to radial distance and the step size to preserve the numerical accuracy (all the calculations were performed on a Digital Equipment Corporation VAX11/780 machine in double precision). In order to obtain fully converged DCS's, we need a larger number of partial waves. We used $l_{\max}$ values [Eqs. (16)–(19)] from 10 to 400. It was found that the present higher-order VPA phase shifts ($l\geq 20$) agree within 0.1% accuracy with the polarized Born calculations[59] using only the asymptotic form of the polarization potential. In all cases the cross sections presented are well converged with respect to increasing $l_{\max}$ and, where required, we switched from VPA phase shifts to polarized Born ones. We now discuss our low-energy results in the 0.1–1 and 2–20-eV regions in subsections III A and III B, respectively. The results at the 20–500-eV range are described in subsection III C.

A. The RT minimum region

In this lower-energy region, the imaginary part [$V_{\rm abs}(r)$] of the optical potential does not play any role.

Very recently, we[23] have explored e-CH_4 scattering in the 0.1–1.0-eV region using various model potentials in the close-coupling approach; it was found that the static-exchange (HFEGE)-polarization (Jain-Thompson[4]) (SEPJT) model (note that in this work orthogonalization[55] is also included in the HFEGE approximation) is too weak to let the RT minimm occur at the right position. The SEPGT model with $r_c=1.175$ [Eq. (6)] gave a good

description of σ_t and σ_m cross sections in this energy domain. In order to see the RT minimum behavior of the present calculations, we show in Fig. 3 our s- and p-wave phase shifts in SEPJT and SEPGT models. Clearly. the SEPJT curve fails to make the s-wave phase shift a multiple of π around 0.4—0.5 eV. Note that the AAHFEGE potential is too strong to give any sensible results in this energy region (not shown). Figure 4 displays our partial and total cross sections along with the experimental σ_t results of Refs. 17 and 19 and our close-coupling results from Ref. 23. The present curve is almost indistinguishable from the close-coupling curve at all energies. The shape of the theoretical and experimental curves agrees qualitatively. It is, however, interesting to note that below about 0.2 eV, our calculated values for the σ_t are in total agreement with recent experimental total cross sections.[17,19] The vibrational excitation threshold in methane is at 0.17 eV.[40] Above this threshold the experimental cross sections are larger than the present ones and the difference between the theory and experiment may be attributed to the threshold vibrational effects. The difference function $[\Delta\sigma_t = \sigma_t(\text{experiment}) - \sigma_t(\text{theory})]$ has certain features of low-energy inelastic scattering due to vibrational excitation effects. A similar behavior of total cross sections below 1 eV has recently been found in the CMS calculations[28(b)] for e-CH_4 scattering. In view of the approximate descriptions of exchange and polarization effects, this qualitative agreement is encouraging.

McKoy and co-workers[60] have extended their Schwinger multichannel calculations[29] for e-CH_4 scattering in the RT minimum region. Remember that their theory treats exchange exactly. In these recent results below 1 eV, polarization effects have been included via the inclusion of closed channels in the expansion of the wave function. Their preliminary results indicate the RT minimum around 0.1 eV; this reflects that the results are not converged, i.e., the polarization is weak. It would be interesting to see their converged results in this low-energy region as compared to our cross sections.

A more stringent test of any model calculation is the comparison of theoretical and experimental DCS's. In this range Müller *et al.*[46] have measured rotationally elastic DCS's for e-CH_4 collisions. We see from Fig. 5 that the two sets of data are in fair agreement qualitatively. However, the experimental points are obtained by fitting their energy loss spectrum to theoretical approximation. Therefore, some quantitative difference between theory and experiment is not clear. In Table I, we give our final data on σ_t, σ_m and DCS in the 0.1—1.0-eV region.

It may be interesting to estimate the scattering length

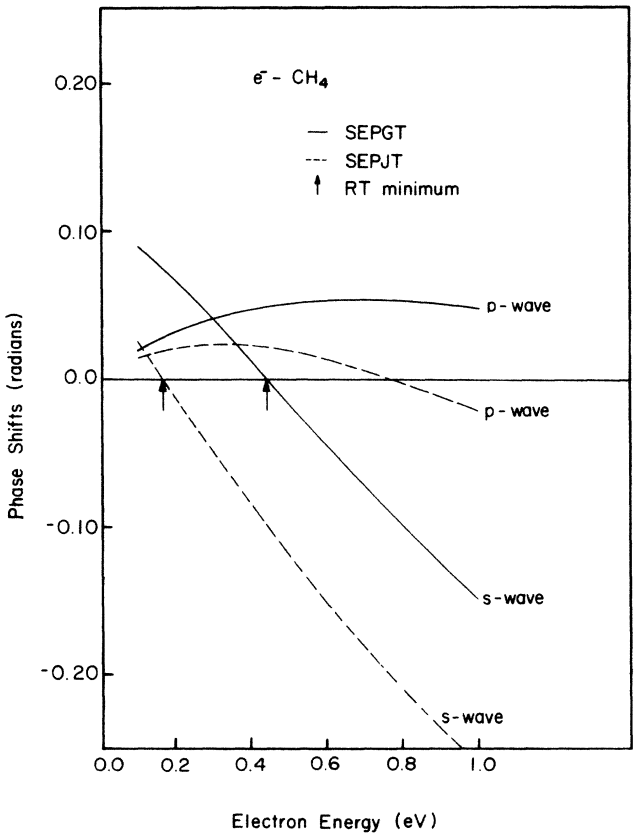

FIG. 3. The s- and p-wave phase shifts for e-CH_4 elastic scattering below 1 eV. Note that the zero phase shift indicates the position of the RT minimum in the s wave. The p-wave zero in the SEPJT model (for notations see the Appendix) is not important. All the curves are labeled according to the approximation.

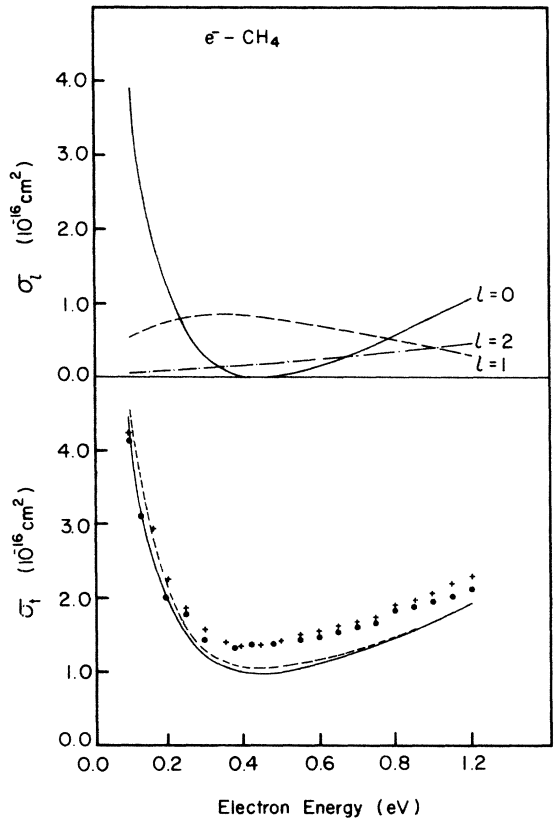

FIG. 4. Partial (upper figure, for s, p, and d waves) and total cross sections for e-CH_4 scattering. The curves of the upper figure are labeled. For the lower (σ_t) figure: present calculations; SEPGT, solid line; SEPJT (Ref. 23), dashed curve. Experimental points are due to: ●, Ref. 19; +, Ref. 17.

(a_0) of e-CH_4 scattering by calculating the phase shift in the zero energy limit. Recently Ferch *et al.*[17] evaluated a_0 (-2.48 a.u.) by extrapolating their measured values towards lower energies. Bloor and Sherrod[28(b)] found a_0 to be -2.47 a.u. from their CMS s-wave phase shifts. We[23] also calculated recently a_0 to be -3.41 a.u. in the SEPGT model using the CC approach. In Table II, we have compared the s-wave phase shifts and partial cross sections (up to 0.001 eV) in the present spherical and the CC calculations. It is not surprising that the two sets of data are in very good agreement. By extrapolating further our s-wave phase shifts towards the zero energy limit, we obtain a_0 to be -3.2 a.u., which is in reasonably good accord with our CC value.[23]

B. Results in the 2–20-eV energy region

Let us discuss first our partial cross sections for the s, p, d, and f waves in various approximations. In Fig. 6, we see that the SEAPJT curve for the d wave is the one which gives the structure around 7–8 eV. It is clear from this figure that the effects of polarization and exchange are important for all partial waves. The total cross sections are plotted in Fig. 7 for various models. We see that the σ_t is very sensitive to exchange and polarization effects together in this range. In general, the AAHFEGE approximation is stronger than the usual HFEGE potential.[55] Notice that the static-exchange (AAHFEGE) approximation (SEAA) curve in Fig. 8 is attractive enough to give a much broader d-wave effect approximately at 10–11 eV without any polarization potential. It is interesting that the static-exchange Schwinger multichannel

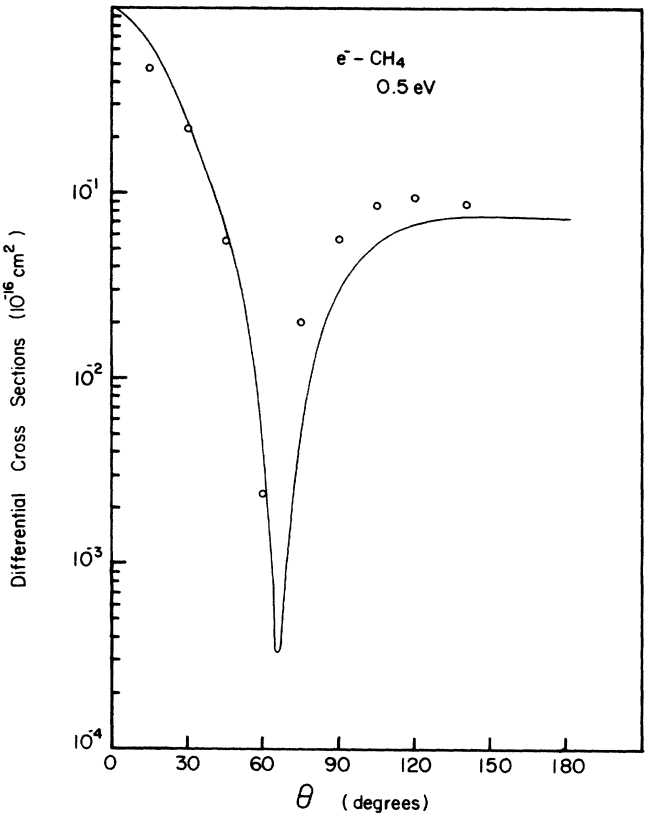

FIG. 5. Differential cross sections for e-CH_4 collisions at 0.5 eV. Solid curve shows present results in the SEPGT model, while open circles are the measurements of Müller *et al.* (Ref. 46) for the rotationally elastic case. For notations see the Appendix.

TABLE I. Differential cross sections for e-CH_4 elastic scattering at 0.1–1.0 eV in the SEPGT model (in units of 10^{-16} cm^2).

Angle (deg)	Energy (eV) 0.1	0.3	0.4	0.5	0.7	1.0
0	1.23	1.06	1.02	0.99	0.95	0.92
5	1.21	1.03	0.98	0.94	0.88	0.84
10	1.18	0.95	0.88	0.81	0.71	0.64
15	1.13	0.83	0.73	0.65	0.52	0.43
20	1.07	0.69	0.58	0.49	0.35	0.27
30	0.91	0.45	0.33	0.25	0.14	0.078
40	0.75	0.28	0.18	0.11	0.037	0.0074
50	0.60	0.16	0.084	0.037	0.016	0.011
60	0.48	0.089	0.03	0.0048	0.0098	0.054
70	0.39	0.042	0.0055	0.000 93	0.038	0.107
80	0.31	0.015	0.000 035	0.012	0.072	0.153
90	0.26	0.003	0.0047	0.028	0.101	0.183
100	0.21	0.000 014	0.014	0.045	0.12	0.194
110	0.17	0.0015	0.024	0.058	0.128	0.188
120	0.14	0.0053	0.034	0.067	0.128	0.171
130	0.12	0.0097	0.041	0.072	0.121	0.148
140	0.11	0.014	0.045	0.075	0.112	0.125
150	0.094	0.017	0.048	0.075	0.103	0.105
160	0.086	0.020	0.050	0.074	0.095	0.089
170	0.081	0.021	0.051	0.074	0.089	0.080
180	0.080	0.020	0.051	0.073	0.088	0.077
σ_t	4.47	1.23	1.01	1.02	1.30	1.71
σ_m	2.65	0.31	0.44	0.69	1.26	1.77

TABLE II. e-CH_4 s-wave scattering below 0.10 eV. The corresponding numbers are from the close-coupling calculations of Jain (Ref. 23) for the A_1 symmetry.

Energy (eV)	Phase shifts (radians) Present	Phase shifts (radians) Jain (Ref. 23)	Partial cross sections (10^{-16} cm^2) Present	Partial cross sections (10^{-16} cm^2) Jain (Ref. 23)
0.001	0.0202	0.0216	19.46	22.23
0.01	0.057	0.058	15.51	15.95
0.025	0.077	0.078	11.34	11.44
0.05	0.089	0.091	7.51	7.56
0.10	0.090	0.093	3.90	3.96

calculations of Lima *et al.*[29] also produce a broad maximum approximately 10–12 eV. Their results (open circles in Fig. 6) are somewhat higher than the present SEAA model. The effect of the JT polarization potential in this static-exchange (SEAA) approximation is to shift the maximum at lower energies in agreement with experimental findings; thus making this model (SEAPJT) superior to all other combinations (Fig. 8).

A real comparison of our total cross sections (only SEAPJT and SEPJT results shown) is made in Fig. 8, where several recent experimental[15–20] and theoretical results[4,25] are also plotted. It is clear from this figure that on an average the SEAPJT calculations are in very good accord with all the experimental data (particularly with the measurements of Refs. 16–19) shown in the figure. The measurements of Kauppila *et al.*[15] are too large around the 7–8-eV structure than the other experimental points (Fig. 8). The SEPJT curve is very close to the CC calculations of Jain and Thompson,[4] who use a similar combination of model potentials except that the orthogonalization[55] is also included along with the HFEGE approximation. We argue that a new CC calculation with AAFEGE (plus the orthogonalization) potential will give better results than the present SEAPJT model. The broad structure is reproduced surprisingly well without involving any adjustable parameter in this range.

We now illustrate our DCS's at 5, 10, and 15 eV along with available experimental and theoretical data in Figs. 9 and 10. The shape of the DCS is mainly dominated by the d-wave scattering, which diminishes as the energy increases (see Figs. 9 and 10). The DCS's at 5 eV are characterized by two forward and backward peaks and two minima at 120° and 50°: in theory (present and close-coupling results of Ref. 4) the later minimum occurs around 30°. At this low energy our SEAPJT DCS's compare reasonably well with the experiment[36,37] and the CC

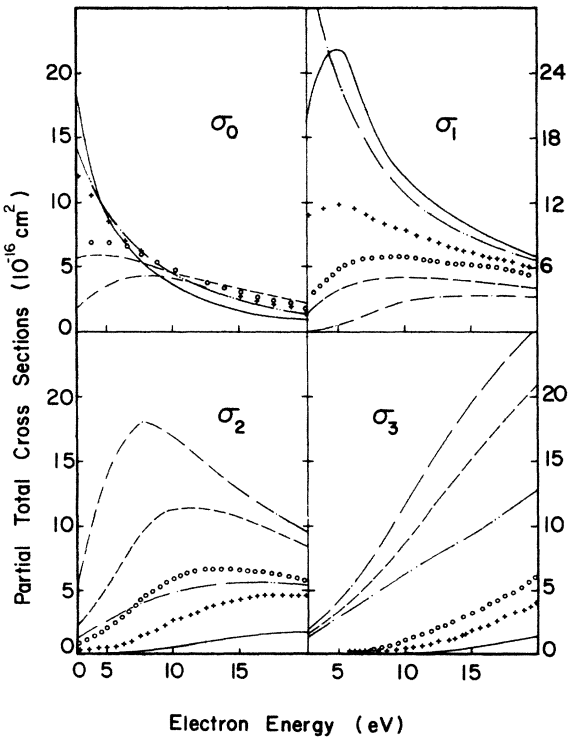

FIG. 6. Partial cross sections for e-CH_4 scattering at 2–20 eV in various models. The four sets of curves are for the s, p, d, and f waves. S, ——; SP —··—··—; SEPTJ, – – – –; SEAPJT, —·—·—; SE, +; SEAA, ○. (For notations see the Appendix.)

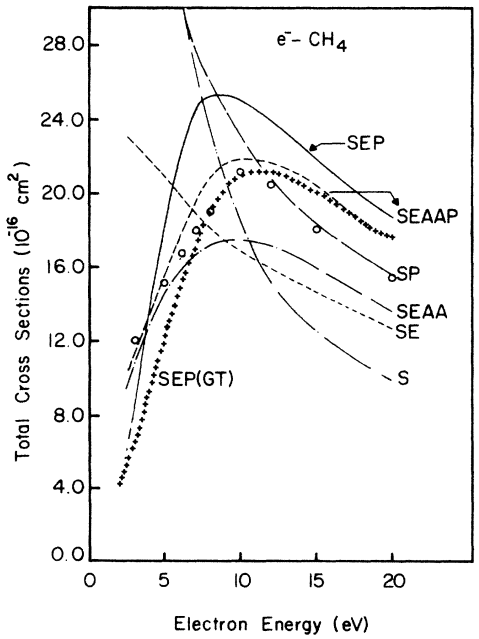

FIG. 7. Total cross sections for e-CH_4 collisions at the 2–20-eV region in various approximations. For all notations see the Appendix. Open circles are the exact exchange (without polarization) calculations of McKoy and co-workers (Ref. 29).

calculations.[4] Above 5 eV the lower angle minima moves to higher angles and becomes a shoulderlike structure around 60°. The present calculated DCS reproduce all the four features, i.e., the backward and the forward peaks, broad shoulder around 60°, and a deep minimum around 120° in fair agreement with experimental DCS. We have not shown the calculations of Bloor,[28] Gianturco *et al.*,[24] and Abusalbi *et al.*[25] (only at 10 eV by the later authors) due to crowded curves in these figures; however, all these rigorous calculations are in good agreement with our spherical approximation results. The results of Lima *et al.*[29] agree only at large angles, since they neglect polarization which describes small-angle scattering. It is really surprising that the present simple model works so well in this low-energy region that it reproduces all the salient features in the e-CH_4 σ_t and DCS.

The only significant difference between the present and the experimental DCS is observed at the second minima beyond 5 eV, where our DCS curves display a very sharp dip at 120° in contrast to a less-pronounced experimental dip: This is due to the fact that the rotationally inelastic DCS's are zero in our work. We can, however, compare our DCS's with the rotationally elastic measurements of Müller *et al.*[46] It is clear from this comparison that in fact rotationally elastic DCS's have a much deeper minimum at middle angles.

A more interesting plot of the present DCS is made in Fig. 11 as a function of energy at few angles. Note that the overall shape and behavior of these curves are very close to a similar plot of experimental DCS's by Tanaka *et al.*[37] (see their Fig. 2). The 120° curve is almost negligible and the 7—8-eV structure occurs around 60—80 deg in both the theory and experiment. The broad peak (Fig.

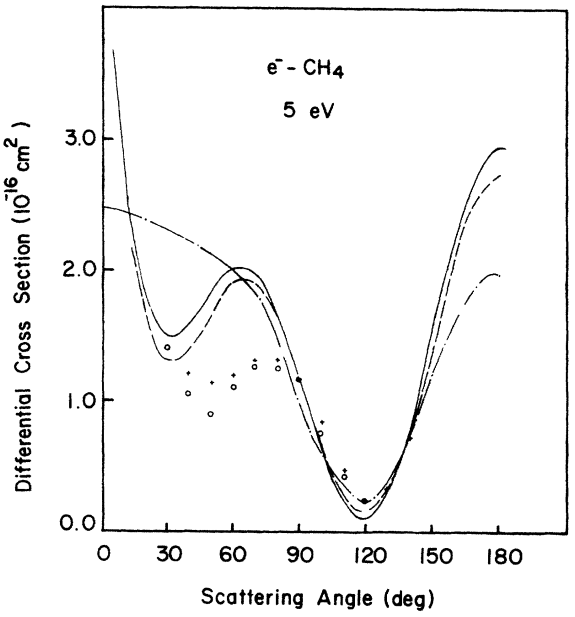

FIG. 9. Differential cross sections for e-CH_4 scattering at 5 eV. Solid curve, present SEAPJT calculations; dashed curve, close-coupling data of Jain and Thompson (Ref. 4). Calculations of McKoy and co-workers (Ref. 29) are shown by dash-dot curve. The experimental points are taken from Ref. 37, +, and Ref. 36, ○.

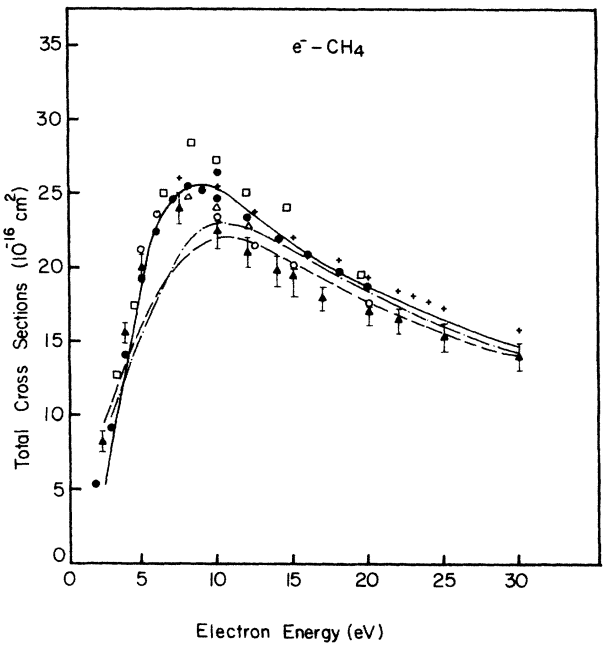

FIG. 8. Total cross sections for e-CH_4 scattering at 2—30 eV shown along with other theoretical and experimental data. Present calculations are shown by the solid (SEAPJT model) and dashed (SEPJT model) curves, while the close-coupling results (Ref. 4) are plotted by the dash-dot curve. At 10 eV, the ⊗ point is the calculated value of Abusalbi *et al.* (Ref. 25). Experimental points: □, Ref. 15; +, Ref. 16; △, Ref. 17; ●, Ref. 19; ▲, Ref. 20.

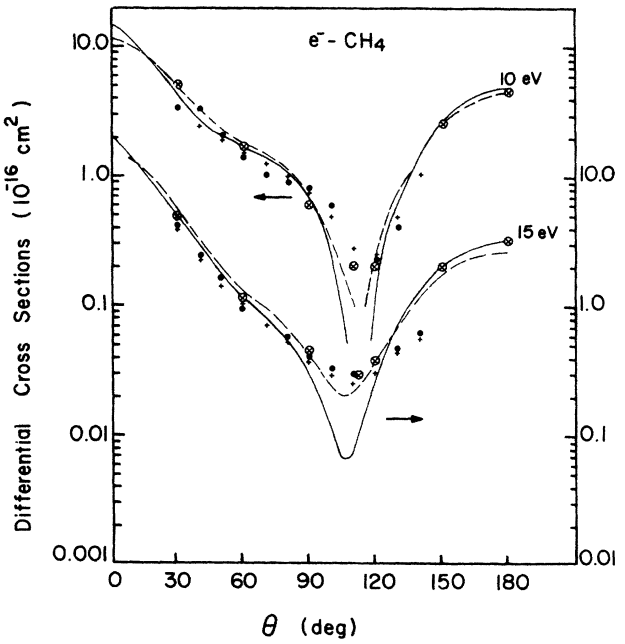

FIG. 10. Same legend as in Fig. 9, but at 10 and 15 eV. The calculations of McKoy and co-workers (Ref. 29) are shown by ⊕.

11) becomes visible, the position of which decreases from about 15 eV at 30° to 5 eV at 110°.

Finally, the σ_m cross sections are evaluated as usual and plotted in Fig. 12 along with experimental data of Refs. 37 and 44. Also shown in this figure are the CC results of Jain and Thompson.[4] The disagreement between our calculations and the data of Refs. 37 and 44 is mainly due the fact that at this energy the swarm analysis[37] may not be accurate and the cross-beam experimental numbers[37] are obtained by extrapolation of their DCS towards lower and higher angles. In addition, the present spherical model is inadequate at larger angles; this may affect our σ_m results in disagreement with other calculations and experimental cross sections. Nevertheless, there is a qualitative agreement between theory and experiment for the momentum-transfer cross sections.

We found that the absorption cross sections are very small in this region. For example, the σ_{abs} at 20 eV contributes only 0.01% to the total cross section. Below 20 eV, the absorption effects are zero. Finally, we give our DCS, σ_t and σ_m values in Table III at several energies in the SEAPJT model.

C. Intermediate- and high-energy regions (20—500 eV)

We first calculate an approximate absorption potential as described in Sec. II [Eq. (7)] and shown in Figs. 1 and 2 at 50 and 400 eV, respectively, by using both $\rho_0(r)$ $[V^0_{abs}(r)]$ and $\rho_1(r)$ $[V^1_{abs}(r)]$. The two curves V^0_{abs} and V^1_{abs} are different with each other but overall shape is similar. The peak in both sets of curves moves towards the center (carbon atom) as the energy increases. At lower energies (Fig. 1) the absorption is mainly from the hydrogen atom surface, while at higher energies (Fig. 2) absorption takes place near the carbon atom.

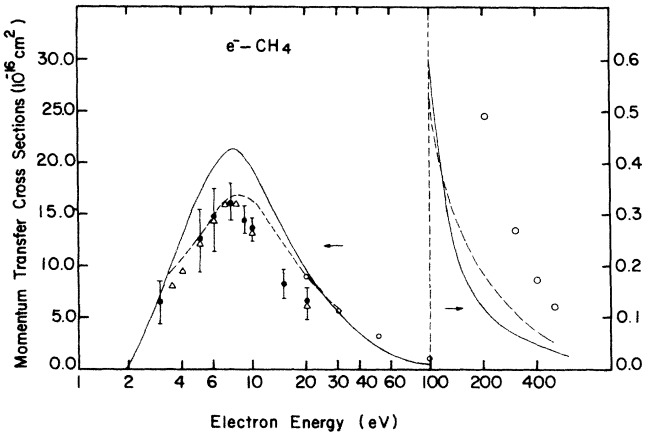

FIG. 12. Momentum-transfer cross sections for e-CH_4 scattering in the 2—500-eV energy region. Solid curve, present calculations in the SEAPJT model (above 20 eV in the SEAPJT$a1$ model); dashed curve (left-hand side), close-coupling results of Jain and Thompson (Ref. 4); dashed curve (right-hand part), present results in the SEAPJT$a0$ approximation. Our previous work (Ref. 2) in the SEPJT model are shown by open circles. Experimental data: swarm data of Ref. 44 are plotted as triangles, while the cross-beam integral numbers of Tanaka *et al.* (Ref. 37) are shown by solid circles.

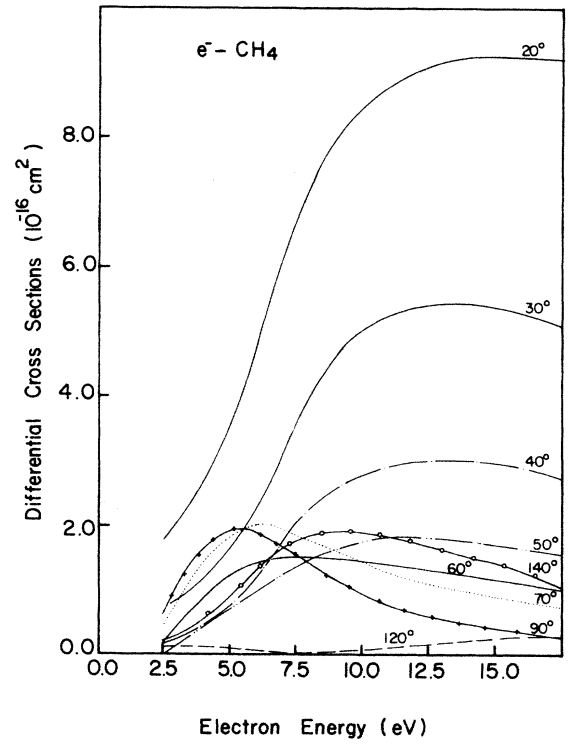

FIG. 11. Differential cross sections for e-CH_4 elastic scattering as a function of energy at 20°, 30°, 40°, 50°, 60°, 70°, 90°, 120°, and 140°. All curves are in the SEAPJT model. For notations see the Appendix.

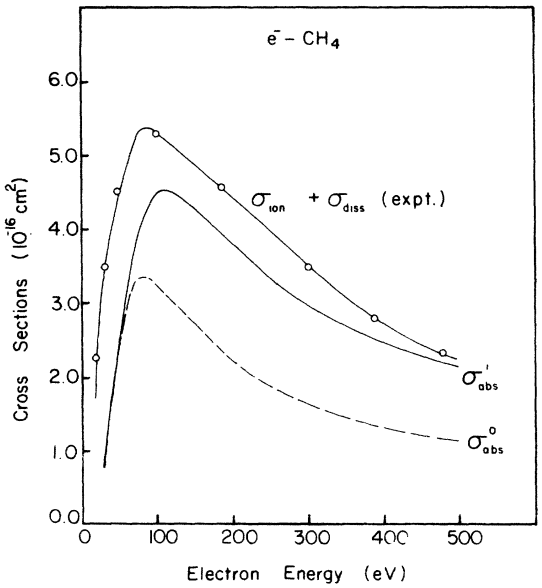

FIG. 13. Absorption cross sections for e-CH_4 scattering above 20 eV. Present results in the SEAPJT$a1$ and SEAPJT$a0$ models are shown, respectively, by a solid line and dashed curves. The open circle, solid line curve is the sum of experimental total dissociation (Ref. 62) and total ionization (Ref. 61) cross sections. For notations see the Appendix.

We first consider σ^0_{abs} and σ^1_{abs} (using V^0_{abs} and V^1_{abs}, respectively) in Fig. 13. A better way to know how reasonable the present absorption potentials are and also which version of the two sets (V^0_{abs} and V^1_{abs}) is more realistic, is to depict in this figure the sum of experimental values of total ionization[61] (σ_{ion}) (without dissociation) and total dissociation[62] (σ_{diss}) cross sections. [Since all excited singlet states of CH_4 are unstable,[63] the cross sections for excitation of methane into a singlet state is included in the σ_{diss} data. And if triplet states are also unstable (although no information is available), the total excitation cross sections are included in the σ_{diss}.] We conclude from Fig. 13 that the σ^1_{abs} is a better approximation. The peak in the σ_{abs} occurs almost at the same place in all the three curves and above 100 eV, the difference between the top two curves is within 15%. In the following we use only the $V^1_{abs}(r)$ potential and consider other potential only for comparison purposes.

We now discuss the effects of absorption potential V^1_{abs} on the unitarity of the S matrix $S_l(k)$. In Figs. 14(a) and 14(b), we show the inelasticity (or the absorption factor) $|S_l(k)|$ as a function of energy for l up to 8. The maximum inelasticity is around 100 eV and then varies slowly with increasing energy indicating that the absorption of the incoming flux is significant. The most affected partial waves are up to $l=6$: The maximum inelasticity is about 0.37 for $l=2$ and 3 around 100–150 eV. For higher partial waves, the absorption factor vanishes rapidly. Since the absorption potential is not of a long-range character, the S matrix is almost unitary for partial waves with $l>15$ up to the highest energy considered here.

In Figs. 15(a) and 15(b), we display the partial cross sections σ^l_{el} and σ^l_{abs} in the elastic (solid curve) and the inelastic (dashed curve) channels, respectively, as a function of energy. The peak in the σ_{abs} curves occurs in almost all partial waves, but the $l=3$–10 waves produce the maximum contribution to the σ_{abs}. The s-wave contribution to the σ_{abs} is very small at all energies and the next p and d waves are small too. The σ^l_{el} dominates over the σ^l_{abs} up to $l=2$ at all energies. However, for higher partial waves ($l>3$), σ^l_{abs} takes over the elastic process above 50 eV. The peak in the σ^l_{abs} around 100 eV is shifted towards higher energies with the increase in l. It is interesting to see, however, that for $l>3$, the σ^l_{el} are also characterized by similar peaks with the same behavior, i.e., the position of the peak moves towards higher l: This is partly due to the fact that the elastic channel couples with the absorption channel. This peaking behavior of the σ^l_{el} exhibits the importance of higher partial waves at higher energies.

A real comparison of our σ_t and experimental data is made in Fig. 16 along with the measurements of Kauppila *et al.*,[15] Floeder *et al.*,[18] Jones,[16] and Sueoka.[20] We have plotted both the σ^1_t (using V^1_{abs}) and σ^0_t (using V^0_{abs}) in this figure. Again the σ^1_t curve is in good accord with the measured data on the average. In this figure we also display the σ^0_{el}, σ^1_{el}, σ^0_{abs}, and σ^1_{abs} cross sections. The crossing point between σ^1_{el} and σ^1_{abs} occurs at 100 eV: however, no such crossing happens between σ^0_{el} and σ^0_{abs} curves. The polarized charge density makes the σ^0_{abs} cross sections larger and, as also seen from Fig. 13, in better agreement with experiment. One more interesting point is worth mentioning here: In the region 60–150 eV, experi-

TABLE III. DCS for e-CH_4 elastic scattering at 2.5–20 eV in the SEAPJT model (in units of 10^{-16} cm^2).

Angle (deg)	Energy (eV) 2.5	5.0	7.5	10.0	12.5	15.0	20.0
0	4.68	9.05	14.36	17.45	19.48	21.16	23.08
5	4.36	8.41	13.29	15.97	17.51	18.63	20.53
10	3.57	6.85	10.96	13.15	14.23	14.92	15.87
15	2.62	5.10	8.67	10.65	11.53	11.92	12.12
20	1.77	3.62	6.78	8.50	9.13	9.29	9.15
30	0.66	1.65	3.79	5.02	5.40	5.36	4.86
40	0.126	0.725	2.04	2.82	3.04	2.96	2.52
50	0.016	0.717	1.41	1.74	1.81	1.72	1.41
60	0.185	1.228	1.50	1.44	1.31	1.17	0.92
70	0.443	1.837	1.82	1.42	1.11	0.89	0.64
80	0.649	2.100	1.89	1.32	0.91	0.66	0.40
90	0.686	1.903	1.56	0.98	0.61	0.41	0.22
100	0.574	1.291	0.90	0.49	0.27	0.18	0.134
110	0.365	0.577	0.25	0.078	0.061	0.10	0.187
120	0.147	0.126	0.024	0.066	0.170	0.27	0.383
130	0.025	0.217	0.51	0.66	0.71	0.73	0.69
140	0.033	0.932	1.76	1.86	1.67	1.45	1.064
150	0.164	2.13	3.55	3.46	2.89	2.30	1.45
160	0.346	3.423	5.39	5.08	4.08	3.11	1.77
170	0.51	4.428	6.80	6.27	4.94	3.69	1.99
180	0.58	4.84	7.29	6.73	5.25	3.91	2.08
σ_t	5.48	18.56	24.93	25.15	23.56	21.73	18.61
σ_m	3.99	16.91	21.35	19.35	16.24	13.54	9.76

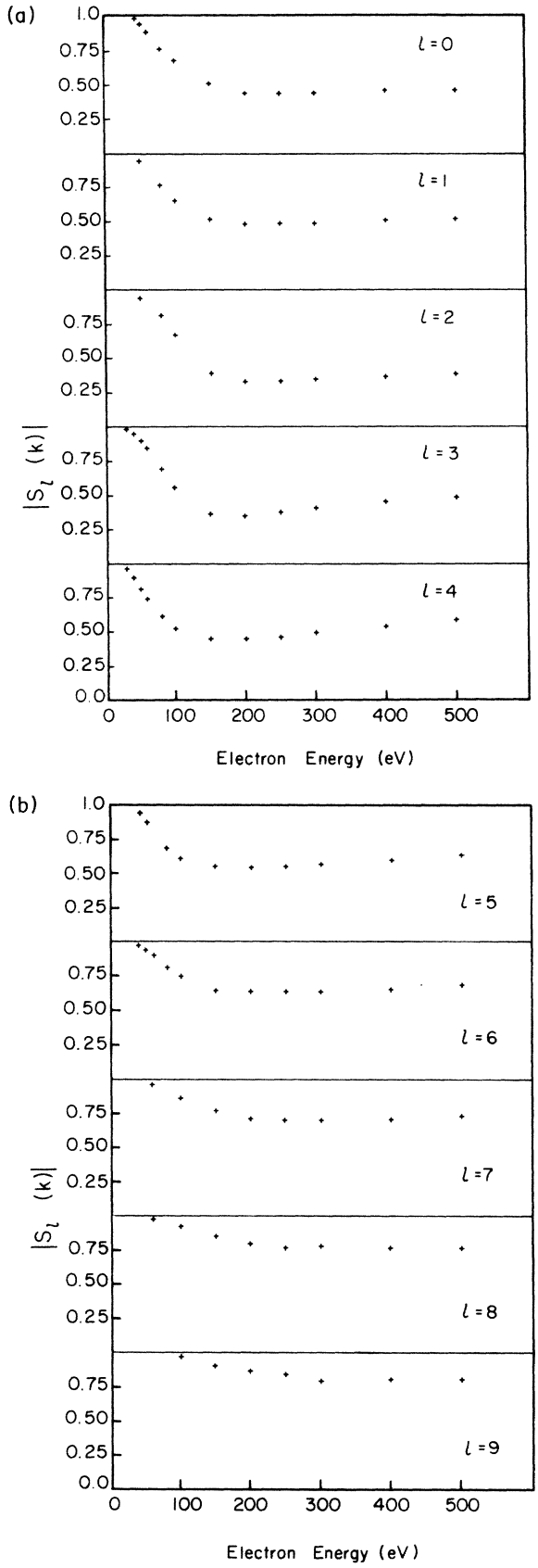

FIG. 14. (a) Absorption factor $|S_l(k)|$ for the e-CH_4 scattering in the 20–500 eV range up to $l=4$. (b) Same as in Fig. 17 but from $l=5$ to 9.

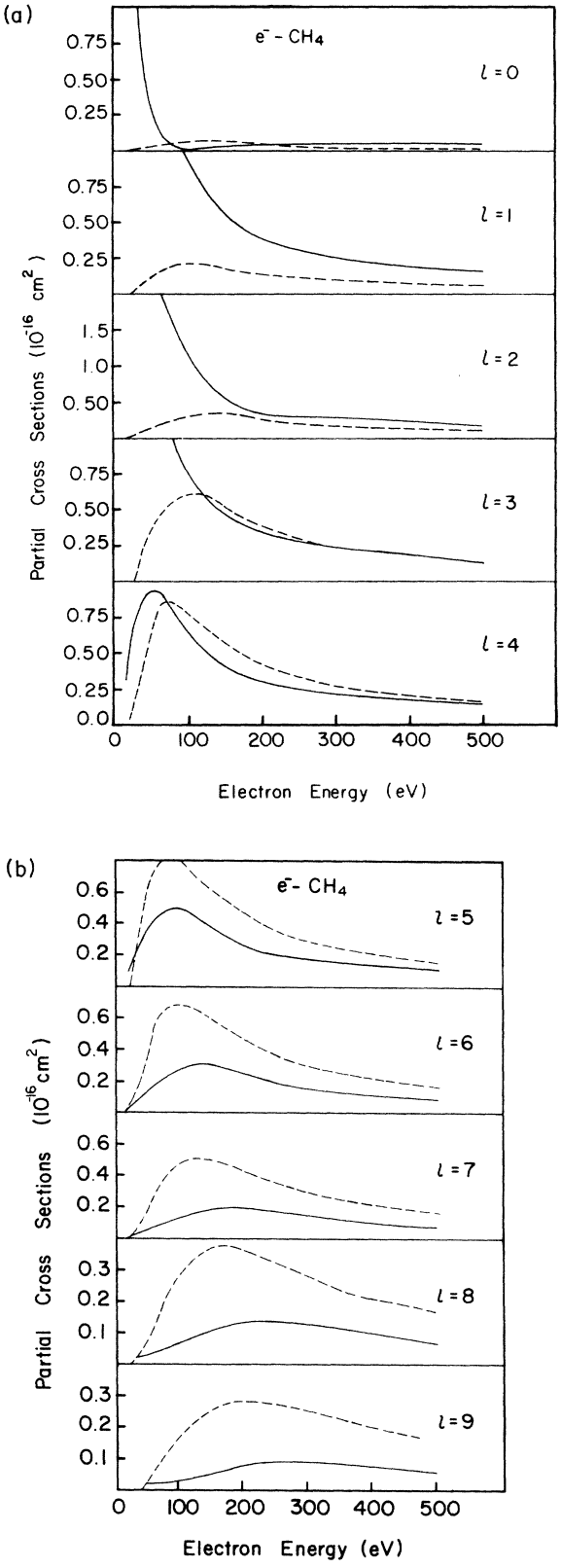

FIG. 15. (a) Partial absorption (dashed curves) and elastic (solid curves) cross sections (in the SEAPJT*a*1 model), for e-CH_4 collisions in the 20–500-eV region. For $l=0$ to 4 only. For notations see the Appendix. (b) Same figure caption as in Fig. 19 but from $l=5$ to 9.

TABLE IV. Elastic cross sections (σ_{el}) for e-CH_4 scattering in various approximations (in units of 10^{-16} cm^2). For notations see the Appendix.

(eV)	SPJTa1	SEa1	SEAa1	SEPJTa1	SEAPJTa1	SEPJT	SEAPJT
30	11.55	9.47	9.99	13.57	14.14	15.60	14.33
40	9.14	7.37	7.69	10.80	11.17	12.80	11.64
50	7.52	5.98	6.20	8.84	9.10	10.85	9.81
60	6.36	5.03	5.18	7.42	7.59	9.40	8.52
80	4.89	3.86	3.93	5.56	5.64	8.00	6.81
100	4.03	3.20	3.23	4.45	4.50	6.46	5.74
150	2.93	2.34	2.35	3.13	3.13	4.80	4.18
200	2.39	1.89	1.89	2.51	2.52	3.74	3.32
300	1.80	1.39	1.39	1.88	1.88	2.71	2.42
400	1.46	1.11	1.11	1.52	1.52	2.13	1.91
500	1.23	0.93	0.93	1.27	1.27	1.75	1.58

mental data indicate a very weak shoulder structure in the σ_t; our σ_t^1 curve also shows such a structure in the same energy region, while the σ_t^0 curve does not reveal such a weak plateau. This is encouraging since the adoption of the polarized charge density is just an *ad hoc* approach to scale the quasifree absorption potential arbitrarily. Although, no attempt has been made to find a best absorption potential surface for the e-CH_4 system.

We now discuss the effects of absorption potential on the elastic scattering. In general, inclusion of the imaginary part in the optical potential reduces elastic cross sections (see Fig. 16). This we demonstrate in Table IV, where σ_{el}^1 (reduced elastic cross sections with V_{abs}^1) values are given in several approximations along with σ_{el} (without absorption). We should compare the last two columns of this table with the fourth and fifth columns, respectively, for this purpose. The lowering of the elastic cross sections due to the imaginary optical-potential part is as much as 35% at 150 eV. Further, this effect is more pronounced in the case of DCS as depicted in Fig. 17 only at 200 and 400 eV. The maximum effect of $V_{abs}(r)$ is at higher angles and at higher energies. The DCS's are reduced by a significant amount particularly at middle angles where in some cases this effect is as much as an order in magnitude. At 50 eV (not shown) the DCS's are decreased beyond a 30° angle, at 200 eV (Fig. 17) above 20°, and at 400 eV (Fig. 17) above 10°. A similar trend in the DCS lowering due to absorption is seen for rare gases.[47] We could not find any experimental data on the absolute DCS above 50 eV to compare with our results. However, for future experimental normalization purposes, we give

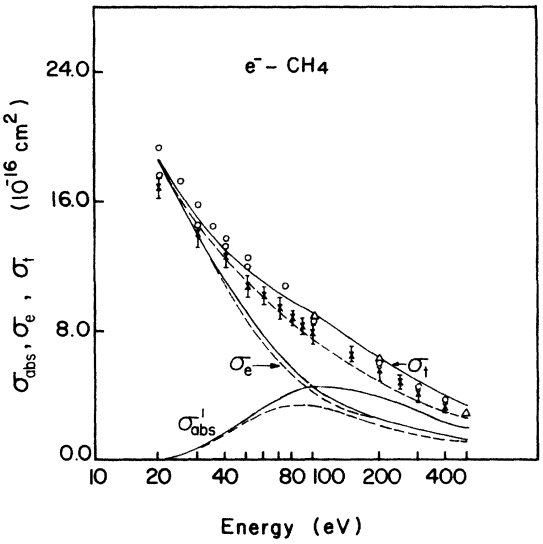

FIG. 16. Total, elastic, and absorption cross sections for e-CH_4 scattering in the 20–500-eV energy range along with the total measurements of Ref. 16 (open circle), Ref. 18 (solid circles), Ref. 15 (triangles) and Ref. 20 (asterisks). The solid and the dashed curves represent present calculations in the SEAPJTa1 and SEAPJTa0 models, respectively. The dashed curve lies just below the corresponding solid curve. All the three cross sections are labeled accordingly. For notations see the Appendix.

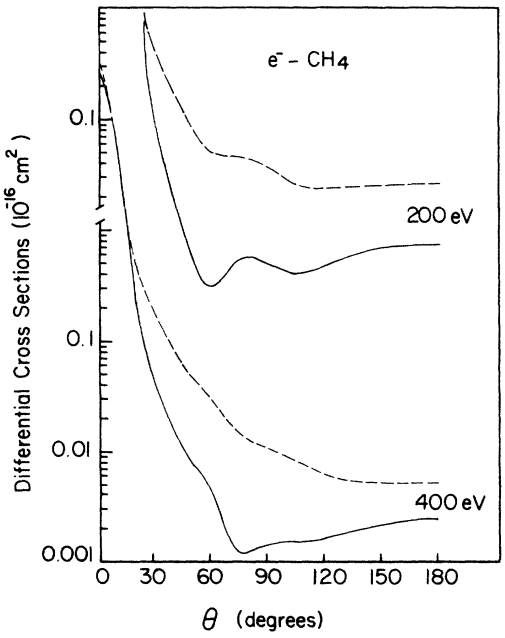

FIG. 17. Differential cross sections for e-CH_4 collisions in the SEAPJT (dashed curve) and SEAPJTa1 (solid curve) models at 200 and 400 eV. For notations see the Appendix.

all our DCS values in Table V with and without absorption.

The σ_m results obtained from the above reduced DCS are illustrated in Fig. 12 along with the pure elastic points taken from Jain.[2] As expected, one can see that the σ_m are reduced considerably due to absorption effects. No experimental information is available for this parameter in this energy range.

We make a few more comments about σ_{abs}. The absorption cross sections are not sensitive to various models of the real part of the complex optical potential (see Table VI). Finally the σ_t^1 is not much sensitive to the exchange approximation (i.e., HFEGE or AAHFEGE) above 100 eV. Nevertheless, the exchange interaction cannot be neglected below 100 eV. For example, at 80 eV, the exchange potential changes the total cross section by about 10%. Similarly, polarization is also effective in this few hundred eV energy region (see Table VII).

IV. CONCLUDING REMARKS

We presented e-CH_4 scattering cross sections in a wide energy range (0.1—500 eV) by using a very simple spheri-

TABLE V. DCS for the e-CH_4 scattering in the SEAPJT (denoted by SEP) and SEAPJTa1 (denoted by SEPa) cases. The latter model indicates the reduced DCS due to inclusion of absorption potential. All numbers are in units of 10^{-16} cm^2. For notations see the Appendix.

	Energy (eV)							
Angle	30		50		60		80	
(deg)	SEP	SEPa	SEP	SEPa	SEP	SEPa	SEP	SEPa
0	28.75	28.96	32.76	32.41	34.32	33.20	36.12	33.26
5	22.41	22.68	23.42	23.66	23.33	23.27	22.88	22.1
10	16.44	16.71	15.48	15.95	14.80	15.19	13.45	13.64
15	11.75	11.94	9.86	10.21	8.97	9.28	7.50	7.67
20	8.16	8.25	6.03	6.10	5.20	5.20	3.96	3.82
30	3.67	3.60	2.07	1.76	1.62	1.22	1.09	0.61
40	1.65	1.55	0.82	0.51	0.65	0.294	0.47	0.108
50	0.90	0.84	0.50	0.32	0.41	0.21	0.294	0.088
60	0.60	0.57	0.33	0.256	0.261	0.170	0.162	0.070
70	0.39	0.38	0.19	0.152	0.136	0.099	0.077	0.045
80	0.215	0.20	0.09	0.067	0.066	0.044	0.044	0.027
90	0.115	0.105	0.06	0.04	0.049	0.029	0.043	0.023
100	0.120	0.115	0.078	0.063	0.064	0.047	0.057	0.033
110	0.217	0.213	0.124	0.115	0.096	0.084	0.079	0.050
120	0.359	0.354	0.181	0.175	0.139	0.126	0.105	0.068
130	0.505	0.498	0.243	0.232	0.189	0.168	0.133	0.086
140	0.626	0.616	0.307	0.282	0.243	0.204	0.160	0.102
150	0.710	0.700	0.370	0.322	0.296	0.234	0.185	0.115
160	0.761	0.749	0.423	0.352	0.341	0.256	0.203	0.126
170	0.787	0.774	0.459	0.371	0.371	0.270	0.215	0.133
180	0.792	0.780	0.471	0.376	0.381	0.274	0.219	0.135
	100		200		300		400	
0	37.18	32.83	39.89	33.88	41.56	36.25	42.59	37.78
5	22.24	20.93	19.07	17.79	16.74	16.07	14.85	14.44
10	12.24	12.23	8.06	8.10	5.79	5.85	4.35	4.32
15	6.33	6.39	3.15	3.02	1.89	1.67	1.26	1.01
20	3.11	2.86	1.25	0.92	0.72	0.423	0.496	0.252
30	0.81	0.334	0.37	0.092	0.24	0.532	0.181	0.044
40	0.38	0.055	0.17	0.017	0.108	0.0156	0.08	0.0163
50	0.22	0.038	0.08	0.0054	0.058	0.0068	0.047	0.0086
60	0.106	0.027	0.05	0.0032	0.045	0.0057	0.031	0.0048
70	0.053	0.021	0.043	0.0048	0.033	0.004	0.018	0.0018
80	0.04	0.019	0.045	0.0058	0.022	0.0021	0.013	0.0020
90	0.047	0.021	0.037	0.005	0.016	0.0018	0.011	0.0015
100	0.061	0.026	0.029	0.0043	0.015	0.0022	0.0096	0.0016
110	0.075	0.032	0.025	0.0043	0.014	0.0028	0.0077	0.0016
120	0.087	0.037	0.024	0.005	0.013	0.003	0.0065	0.0016
130	0.097	0.043	0.025	0.0058	0.012	0.0031	0.0059	0.0018
140	0.105	0.049	0.025	0.0066	0.011	0.0031	0.0057	0.0021
150	0.112	0.055	0.026	0.0071	0.0098	0.0032	0.0056	0.0023
160	0.117	0.061	0.027	0.0074	0.0093	0.0033	0.0055	0.0025
170	0.120	0.064	0.027	0.0076	0.0090	0.0033	0.0055	0.0025
180	0.121	0.066	0.027	0.0077	0.0089	0.0034	0.0055	0.0026

TABLE VI. σ_{abs}^{1} (using V_{abs}^{1} absorption potential) in various approximations for e-CH_4 scattering (in units of 10^{-16} cm^2).

(eV)	SPJTa1	SEa1	SEAa1	SEPTJa1	SEAPJTa1
30	0.712	0.696	0.697	0.710	0.710
40	1.667	1.630	1.640	1.661	1.660
50	2.540	2.500	2.500	2.538	2.540
60	3.260	3.210	3.210	3.258	3.260
80	4.150	4.100	4.100	4.161	4.170
100	4.480	4.435	4.440	4.498	4.500
150	4.280	4.242	4.240	4.292	4.290
200	3.790	3.761	3.760	3.795	3.795
300	3.020	3.010	3.010	3.030	3.030
400	2.510	2.500	2.500	2.520	2.520
500	2.150	2.150	2.150	2.150	2.150

cal model. This model involves no adjustable parameter, except below 1 eV, where in order to reproduce the RT minimum, we adopt a parameter-dependent form of the polarization potential. In the 2–20-eV region, the present parameter-free approximation gives a broad shape resonancelike structure around 7–8 eV, which is in very good agreement with recent measurements. In addition, the present model reproduces all the structures observed in the experimental DCS and very close to previous close-coupling, MS$X\alpha$,[26–28] and Schwinger multichannel calculations. The only difference occurs in the DCS at 120°, where the present results should be compared with rotationally elastic measurements of Müller *et al.*[46]

The inclusion of an absorption potential as the imaginary part of the total optical potential makes it possible to compare our total (elastic plus absorption) cross sections with several recent experimental data in the 20–500-eV range. We also discuss the unitarity of the S matrix in terms of the inelasticity or the absorption factor. The shape of the present absorption cross sections is in good accord with the experimental sum of total dissociation and ionization cross sections for methane by electron impact. The absorption cross sections are peaked around 100 eV and larger than the elastic ones beyond this energy. The effect of the absorption potential is to reduce the elastic cross sections (σ_t, σ_m, and the DCS) significantly.

We have also updated theoretical and experimental work on e-CH_4 collisions until 1986.

We finally conclude that a spherical description of the e-CH_4 system is quite adequate to yield reliable cross-section parameters from a very low to very high energy region. And if the combination of model exchange and polarization potentials is made correctly, or alternatively, if the two interactions are included very accurately, the spherical model is capable of reproducing almost all the observed structures in the σ_t (RT minimum, 7–8 eV broad resonance due to d wave and a broad shoulder around 60–150 eV), DCS (below 20 eV a sharp minimum at 120° and a shallow structure around 30–60 deg), and the σ_m (same as in the σ_t). However, below 1 eV, the RT minimum is forced to occur by tuning a parameter-dependent polarization potential. This is mainly due to the inadequacy of present model local exchange and polarization potentials to represent the true nature of such forces in this very low-energy domain. In their recent multichannel Schwinger variational calculations, McKoy and co-workers[60] have been successful at observing this minimum. Their preliminary results with a small number of polarization channels show the RT minimum around 0.1 eV, which is too low with respect to the experimental position; however, it is expected that their final calculations, with converged polarization effects, should improve

TABLE VII. Total cross sections in various models for e-CH_4 collisions in units of 10^{-16} cm^2 (for notations see the Appendix).

(eV)	SPJTa1	SEAa1	SEa1	SEPJTa1	SEAPJTa1
30	12.26	10.69	10.17	14.28	14.85
40	10.81	9.33	9.00	12.46	12.84
50	10.06	8.70	8.48	11.38	11.64
60	9.62	8.39	8.24	10.68	10.85
80	9.04	8.04	7.96	9.72	9.81
100	8.51	7.67	7.63	8.95	9.00
150	7.21	6.59	6.58	7.41	7.42
200	6.18	5.65	5.65	6.31	6.32
300	4.83	4.40	4.40	4.91	4.91
400	3.98	3.62	3.61	4.03	4.03
500	3.39	3.07	3.07	3.43	3.43

upon this low value of 0.1 eV.

This model cannot give information on the rotational excitations. However, one can pursue this theory further to study vibrational excitations in methane molecules due to slow electron impact.

All the conclusions made here regarding the use of various approximate potentials for e-CH_4 scattering are also valid in a model potential close-coupling approach.

It may be worth it to test this model for a heavier system. For example, the SiH_4 molecule, where a much stronger maximum in the total cross section is observed around 2—3 eV, again due to the d-wave scattering. Our preliminary results on the e-SiH_4 total cross sections[64] indicate that a spherical model is quite promising for such a highly polarizable and symmetrical polyatomic molecule.

Note added in proof. Very recently, we came to know that Gianturco and Scialla[65] have used a parameter-free model potential approach in the one-center close-coupling formalism[22] to study e-CH_4 collisions below 20 eV. They have introduced a modified version of the usual semiclassical-exchange potential along with a parameter-free correlation-polarization term. In particular, their total cross sections exhibit the RT effect in good qualitative agreement with the experimental data.

ACKNOWLEDGMENTS

This calculation was started at the Joint Institute for Laboratory Astrophysics (JILA), University of Colorado and National Bureau of Standards, Boulder, CO. I am thankful to Dr. D. G. Thompson and Professor F. A. Gianturco for reading this manuscript and making helpful comments. The final calculations were completed on the VAX11/750 computer at the Physics Department, Kansas State University. I am grateful to Professor W. E. Kauppila, Dr. G. Sinapius, Dr. S. J. Buckman, and Dr. O. Sueoka for sending their experimental data in tabular form. Finally my thanks also extend to Professor C. P. Bhalla and Professor C. D. Lin for providing research facilities to complete this work.

APPENDIX: GLOSSARY OF ABBREVIATIONS USED IN THE TEXT

If we denote static and exchange terms by capital letters S and E, respectively, and the polarization term by PJT (due to Jain and Thompson,[4] JT potential) and PGT [due to Gianturco and Thompson,[21,22] GT potential; Eq. (6)], then:

SE is S plus HFEGE potential;
SEAA is S plus AAHFEGE potential;
SPGT is S plus GT polarization [Eq. (6)];
SPJT is S plus JT polarization (Ref. 4);
SEPGT is SPGT plus HFEGE potential;
SEAPGT is SPGT plus AAHFEGE potential;
SEPJT is SPJT plus HFEGE potential;
SEAPJT is SPJT plus AAHFEGE potential.

In order to denote the above terms with absorption potential, we add extra letters $a0$ and $a1$ depending upon the V_{abs} (0 or 1). For example,

SEAPJT$a0$ is SEAPJT with $V^0_{abs}(r)$;
SEAPJT$a1$ is SEAPJT with $V^1_{abs}(r)$.

[1]A. Jain, J. Chem. Phys. **78**, 6579 (1983).
[2]A. Jain, J. Chem. Phys. **81**, 724 (1984).
[3]S. Hara, J. Phys. Soc. Jpn. **22**, 710 (1967).
[4]A. Jain and D. G. Thompson, J. Phys. B **15**, L631 (1982).
[5]A. Jain and D. G. Thompson, J. Phys. B **16**, 3077 (1983).
[6]R. A. Buckingham, H. S. W. Massey, and S. R. Tibbs, Proc. R. Soc. London, Ser. A **178**, 119 (1940).
[7]S. S. Dhal, B. B. Srivastava, and R. Shingal, J. Phys. B **12**, 2727 (1979).
[8]C. Ramsauer and R. Kollath, Ann. Phys. (Leipzig) **4**, 91 (1930).
[9]E. Brüche, Ann. Phys. (Leipzig) **4**, 387 (1930).
[10]R. B. Broad, Phys. Rev. **25**, 636 (1925).
[11]E. Brüche, Ann. Phys. (Leipzig) **83**, 1065 (1927).
[12]E. Barbarito, M. Basta, M. Calicchio, and G. Tessari, J. Chem. Phys. **71**, 54 (1979).
[13]D. Mathur, J. Phys. B **13**, 4703 (1980).
[14]T. C. Griffith, M. Charlton, G. Clark, G. R. Heyland, and G. L. Wright, in *The Positron Annihilation,* edited by P. G. Coleman, S. C. Sharma, and L. M. Diana (North-Holland, Amsterdam, 1982), pp. 61—70.
[15]W. E. Kuappila, M. S. Dababneh, Y.-F. Hsieh, Ch. K. Kwan, S. J. Smith, T. S. Stein, and M. N. Uddin, in *Proceedings of the 13th International Conference on the Physics of Electronic and Atomic Collisions, Berlin, 1983,* edited by J. Eichler *et al.* (North-Holland, Amsterdam, 1983), p. 303; also (private communication).
[16]R. K. Jones, J. Chem. Phys. **82**, 5424 (1985).
[17]J. Ferch, B. Granitza, and W. Raith, J. Phys B **18**, L445 (1985).
[18]K. Floeder, D. Fromme, W. Raith, A. Schwab, and G. Sinapius, J. Phys. B **18**, 3347 (1985).
[19]B. Lohmann and S. J. Buckmann, J. Phys. B (to be published).
[20]O. Sueoka (private communication).
[21]F. A. Gianturco and D. G. Thompson, J. Phys. B **9**, L383 (1976).
[22]F. A. Gianturco and D. G. Thompson, J. Phys. B **13**, 613 (1980).
[23]A. Jain, Phys. Rev. A **34**, 954 (1986).
[24]F. A. Gianturco, A. Jain, and L. Pantano, J. Phys. B (to be published).
[25]N. Abusalbi, R. A. Eades, T. Nam, D. Thirumlai, D. A. Dixon, and D. G. Truhalar, J. Chem. Phys. **78**, 1213 (1983).
[26]Zs Varga, I. Gyemant, and M. G. Benedict, Acta Phys. Chem. **25**, 85 (1979).
[27]J. A. Tossel and J. W. Davenport, J. Chem. Phys. **80**, 813 (1984).
[28](a) J. E. Bloor, in *Wavefunctions and Mechanisms from Electron-Scattering Processes,* edited by F. A. Gianturco and G. Stefani (Springer, New York, 1984), p. 85; (b) J. E. Bloor and R. E. Sherrod, J. Phys. Chem. (to be published).
[29]M. A. P. Lima, T. L. Gibson, W. M. Huo, and V. McKoy, Phys. Rev. A **32**, 2696 (1985).
[30]F. A. Gianturco and D. G. Thompson, Comments At. Mol. Phys. **31**, 307 (1985).
[31]F. A. Gianturco and A. Jain, Phys. Rep. (to be published).
[32]E. C. Bullard and H. S. W. Massey, Proc. R. Soc. London,

Ser. A **133**, 637 (1931).
[33]F. L. Arnot, Proc. R. Soc. London, Ser. A **133**, 615 (1931).
[34]C. B. O. Mohr and F. H. Nicoll, Proc. R. Soc. London, Ser. A **138**, 469 (1932).
[35]A. C. Hughes and J. H. McMillen, Phys. Rev. **44**, 876 (1933).
[36]K. Rohr, J. Phys. B **31**, 4897 (1980).
[37]H. Tanaka, T. Okada, L. Boesten, T. Suzuki, T. Yamamoto, and H. Kubo, J. Phys. B **15**, 3305 (1982).
[38]H. Tanaka, M. Kubo, N. Onodera, and A. Suzuki, J. Phys. B **16**, 2861 (1983).
[39]L. Vuskovic and S. Trajmar, J. Chem. Phys. **78**, 4947 (1983).
[40]W. Sohn, K. Jung, and H. Ehrhardt, J. Phys. B **16**, 891 (1983).
[41]P. J. Curry, W. R. Newell, and A. C. H. Smith, J. Phys. B **18**, 2303 (1985).
[42]T. L. Cottrell and I. C. Walker, Trans. Faraday Soc. **61**, 1585 (1965); **63**, 649 (1967).
[43]C. W. Duncan and I. C. Walker, J. Chem. Soc. Faraday Trans. II **68**, 1514 (1972).
[44]G. N. Hadded, Aust. J. Phys. **38**, 677 (1986).
[45]R. Tice and D. Kivelson, J. Chem. **46**, 4743 (1967).
[46]R. Müller, K. Jung, K.-H. Kochem, W. Sohn, and E. Ehrhardt, J. Phys. B **18**, 3971 (1985).
[47]G. Staszewska, D. W. Schwenke, D. Thirumalai, and D. G. Truhlar, J. Phys. B **16**, L281 (1983); Phys. Rev. A **28**, 2740 (1983); G. Staszewska, D. W. Schwenke, and D. G. Truhlar, J. Chem. Phys. **81**, 335 (1984); Phys. Rev. A **29**, 3078 (1984).
[48]A. Jain and D. G. Thompson, J. Phys. B **16**, 1113 (1983).
[49]L. G. Christophrou, S. R. Hunter, J. G. Carter, and R. A. Mathis, Appl. Phys. Lett. **41**, 147 (1982).
[50]L. E. Kline, IEEE Trans. Plasma Sci. **PS-10**, 224 (1982).
[51]G. Schulz and J. Gresser, Nucl. Instrum. Methods **151**, 413 (1978).
[52]V. Palladino and B. Sadoulet, Nucl. Instrum. Methods **128**, 323 (1975).
[53]A. L. Broadfoot *et al.*, Nature **204**, 979 (1979).
[54]F. A. Gianturco and D. G. Thompson, Chem. Phys. **14**, 111 (1976); the one-center wave functions for CH_4 are discussed by R. Moccia, J. Chem. Phys. **40**, 2164 (1964).
[55]S. Salvini and D. G. Thompson, J. Phys. B **14**, 3797 (1981).
[56]*Landolt-Börstein, Zahlenwerte und Functionen*, (Springer-Verlag, Berlin, 1951), Vol. 3, Pt. 3, p. 511.
[57]J. A. Pople and P. Schofield, Philos. Mag. **2**, 591 (1957).
[58]F. Calogero, *Variable Phase Approach to Potential Scattering* (Academic, New York 1974).
[59]T. F. O'Mally, L. Spruch, and L. Rosenberg, J. Math. Phys. **2**, 491 (1961).
[60]M. A. P. Lima, T. L. Gibson W. M. Huo, L. M. Brescansin, Z. Luo, K. Watari, and V. McKoy, Bull. Am. Phys. Soc. **31**, 953 (1986); and private communication from W. M. Huo and V. McKoy.
[61]B. Adamczyk, A. J. H. Boerboom, B. L. Schram, and J. Kistmaker, J. Chem. Phys. **44**, 4640 (1966).
[62]H. F. Winter, J. Chem. Phys. **63**, 3462 (1975).
[63]J. F. M. Aarts, C. I. M. Beenkker, and F. J. de Heer, Physica (Utrecht) **53**, 32 (1971).
[64]A. Jain (unpublished).
[65]F. A. Gianturco and S. Scialla, J. Phys. B (to be published).